Indole-3-carbinol Inhibits Lipopolysaccharides-induced Small Intestinal Inflammation and Metabolic Disorder by Improving Glycerophospholipids Metabolism in Rabbits

Zihan Guo
Southwest University https://orcid.org/0000-0002-1800-3205
Na Zhao
Southwest China Normal University: Southwest University
Wang Cheng Liu
Southwest University
Puran Chen
Southwest China Normal University: Southwest University
Xiang Fu
Southwest University
Bin Wang
Southwest University
Jing Li
Southwest University
Xin Ye
Southwest China Normal University: Southwest University
Jingzhi Lu (ljzzl-66@163.com)
Southwest China Normal University: Southwest University

Research

Keywords: Inflammation, I3C, PPAR pathway, phosphatidylcholine, NOD-like pathway

Posted Date: October 22nd, 2021

DOI: https://doi.org/10.21203/rs.3.rs-978453/v1

Abstract

Background

Indole-3-carbinol (I3C), a natural hydrolysis product of glucobrassicin, has a good effect on cancer, obesity, and inflammatory bowel disease. The objective of this study was to investigate the effect of I3C on small intestinal inflammation induced by LPS in rabbits. 40 rabbits were randomly and averagely divided into four groups: control, I3C (40 mg·kg^{-1}·BW I3C, OP), lipopolysaccharides (LPS) (0.5 mg·kg^{-1}·BW LPS, IP injection), I3C + LPS (40 mg·kg^{-1}·BW I3C, OP; 0.5 mg·kg^{-1}·BW LPS, IP injection). The mRNA expression of pro-inflammatory genes, intestinal injury in jejunum mucosa, the single and combined analysis of jejunum mucosa RNA-seq and serum metabolome were performed to explore the anti-inflammatory mechanism of I3C induced by LPS in rabbits.

Results

I3C group rabbits exerted a higher growth performance and intestinal immunity compared to the control group. In the comparison of I3C+LPS vs. LPS, I3C improved the metabolism of lipid, carbohydrate, vitamins, and increased the contents of serum carboxylic acids and derivatives, glycerophospholipids, steroids and steroid derivatives, fatty acyls, prenol lipids, and organooxygen compounds, which were all decreased by LPS. I3C suppressed the expression of pro-inflammatory genes (TNF-α, IL-1β, IL-6, ICAM1, NOS2, GRO-B) and inhibited NOD-like and JAK-STAT signaling pathway induced by LPS through activating the peroxisome proliferator-activated receptors (PPAR) signaling pathway. From the Weighted Gene Co-expression Network Analysis (WGCNA), we found serum phosphatidylcholine (PC) (16:0/24:1(15Z)) was negatively correlated with NOD-like and JAK-STAT signaling pathway, and positively correlated with PPAR signaling pathway, while PC (20:2(11Z,14Z)/14:0) contrary to it. PC (16:0/24:1(15Z)) was negatively related to secreted phospholipase (sPLA2), but PC (20:2(11Z,14Z)/14:0) was positively regulated by solute carrier family 44 member 4 (SLC44A4). Meanwhile, I3C both reduced the upregulated expression of sPLA2 and SLC44A4, together with the serum restoration of decreased PC (16:0/24:1(15Z)) and increased PC (20:2(11Z,14Z)/14:0) stimulated by LPS.

Conclusion

I3C participated in reducing intestinal inflammation through activating the PPAR signaling pathway and improving glycerophospholipids synthesis and metabolism. We also found PC (16:0/24:1(15Z)) may be a endogenous agonists of PPAR, and PC (20:2(11Z,14Z)/14:0) may be an inflammatory biomarker.

Background

LPS is a potentially toxic compound produced by Gram-negative bacteria and other pathogens like chlamydia [1]. LPS is mainly a component of the outer leaflet of the outer membrane of most Gram-negative bacteria, consisting of polysaccharides and major bioactivity element lipid A [2]. It could be recognized by Toll-like receptor 4 on the macrophages membrane and activated NF-κB signaling pathway to produce inflammatory cytokines (TNF-α, IL-6, IL-1β, etc.), resulting in inflammatory response and damaging intestinal tight junction [3, 4]. The gut is considered an important source of LPS [5]. The gastrointestinal tract is a habitat of gut microbiota (bacteria, virus, archaea, fungi and protozoa) which established bidirectional communication with the host body [6]. Through tryptophan metabolites [7], short-chain fatty acid [8] and bile acids [9], gut bacteria regulated intestinal epithelial innate immune system (immune cells, Innate lymphoid cell 3, regulatory T cells, immune molecule, IL-22, antimicrobial peptides,

etc.) to maintain immune tolerance and intestinal microflora balance [10]. Once intestinal homeostasis is broken, the host will be attacked by chronic intestinal inflammation [11], diarrhea [12], etc. The intestinal barrier dysfunction can drive microbial-derived LPS to penetrate tissue and blood, then LPS is transported into brain barrier through lipoproteins [13], affecting brain function and mental state [14]. Irritable bowel syndrome is typically influenced by intestinal flora imbalance and makes some patients occur with depression and anxiety [15, 16].

The enterotoxigenic Escherichia coli (ETEC) is considered the main pathogen that causes high morbidity and mortality of serious diarrhea in children in poor areas [17], as well as in animal husbandry [18]. The effluent from animal markets may contribute to the spreading of diarrheagenic ETEC in the environment [19]. Scientists had invented tens of thousands of antimicrobials to deal with the popularity of diarrhea caused by ETEC over the past few decades. However, there comes a question of antimicrobial resistance, one of the greatest long-term threats to humans, no less than climate change and terrorism [20]. The Chinese government has introduced a series of policies to prohibit the abuse of antibiotics since the Global Action Plan in 2015 by the WHO. Therefore, finding alternatives to antibiotics will be a major feature of future research.

Indole-3-carbinol (I3C) is a natural compound, hydrolyzed from glucosinolates in brassica vegetables (cabbage, broccoli, cauliflower, sprouts, turnip, kale and kohlrabi) by myrosinase. As a feed additive, I3C could alleviate chicken coccidiosis [21], reduce Citrobacter rodentium adhesion in the colon of mice [22], in which I3C modulated naive T cell differentiation [23, 24] and interfered with the activity of NF-κB to suppress the expression of pro-inflammatory cytokines [25] mainly through AhR signaling pathway. Besides, I3C had a potential cancer chemopreventive effect by suppressing cyclin D1 [26] or changing gut microbial composition [27], prevented mice from DOX-induced toxicities [28] by Nrf2 signaling pathway, suppressed obesity [29] and CCl4-induced hepatic injury [30] by PPAR signaling pathway.

Glycerophospholipids are key components of cellular lipid bilayer, bile and membrane surfactant, participating in protein recognition and signal transduction of cell membrane. Glycerophospholipids can be divided into distinct classes based on the polar “head group” at the sn-3 position of the glycerol backbone in eukaryotes [31], including phosphatidic acid (PA), PC, phosphatidylethanolamine (PE), phosphatidylinositol (PI), glycerol phosphatidylglycerol (PG) and phosphatidylserine (PS), etc. Glycerophospholipids metabolism disorder in cell membrane can lead to inflammatory diseases [32], such as cancer [33], Alzheimer's disease [34], diabetes[35], inflammatory bowel disease (IBD) [36], etc. WU [37]studied the effects of non-steroidal anti-inflammatory drugs on glycerophospholipids constituents in RAW264.7 cells and found PC(16:0/18:1) and PE(18:0/18:1) might be important biomarkers of inflammation. Cifkova [38] determined the lipidomic differences between breast cancer patients and healthy people and detected several PEs decreased in patients. Zhang [39] found PE(18:0/18:1) might be the important glycerophospholipid biomarker in inflammation in the study of anti-inflammation of Alpinia officinarum. In this study, we used both metabolomics and the RNA-seq to investigate the anti-inflammatory effects and mechanism of I3C in small intestinal enteritis on rabbits.

Materials And Methods

Chemicals and biochemicals

I3C (CAS: 700-06-1) and LPS (Escherichia coli O55:B5) were obtained from Sigma Chemical (St Louis, MO, USA), and Dimethyl sulfoxide (DMSO) from BioFroxx (Germany).

Animal experiments

6-week-old male Hyla rabbits were raised in stain-steel cages with a temperature regulation system, and all the groups were fed a basal diet with no antibiotic additives (Table 1). Water and diets were provided *ad libitum*. After a week pre-experiment, 40 rabbits were randomly and averagely assigned to four groups: control, I3C (40 mg·kg^{-1}·BW I3C, OP), LPS (0.5 mg·kg^{-1}·BW LPS, IP injection), I3C+LPS (40 mg·kg^{-1}·BW I3C, OP; 0.5 mg·kg^{-1}·BW LPS, IP injection). In the analysis of RNA-seq and serum metabolome, control, I3C, LPS, I3C+LPS group were named as C, I, L, IL, respectively.

Rabbits were administrated 40 mg·kg^{-1}·BW I3C (dissolved in a solution of 92% corn oil and 8% DMSO) or vehicle (92% corn oil and 8% DMSO) orally for two weeks. At the end of the experiment, rabbits were intraperitoneally injected 0.5 mg·kg^{-1}·BW LPS (dissolved in saline) or saline.

Rabbits were sacrificed four hours later after injection, and the blood and organs were collected for the next assay. All the procedures of animal experiments were approved by the Ethics Committee of Animal Welfare at Southwest University (IACUC Issue No. 20210122-1).

Table 1
Ingredients and nutrient levels of the basal diets (air-dry basis) (%)

Ingredients, %	Content	Nutrient levels, %	Content
Corn	19	DE(KJ/kg)	10.01
Soybean meal	15.19	CP	16.05
Wheat bran	18	EE	2.49
Alfalfa	31	CF	16.15
Corn germ cake	4.2	Ca	0.77
Chaff	7	P	0.41
Wheat middling	2	Lys	0.79
$CaHPO_4$	1.2	Met+Cys	0.60
NaCl	0.3		
Met	0.11		
Glucose	1		
Premix	1		
Total	100		
The premix provided the following per kg of diets: VA 10 000 IU,VD3 1000 IU□VE 30 mg□VK3 1 mg□VB1 1 mg□VB2 3.5 mg□Cu 5 mg□Fe 30 mg□I 1 mg□Se 0.08 mg□Zn 30 mg□Mn 15 mg□			

Growth performance

The body weight and feed intake were recorded each day and then calculated average daily gain (ADG), average daily feed intake (ADFI) and feed conversion ratio (FCR).

Intestinal morphology analysis

Jejunum tissues were sampled and fixed in 4% paraformaldehyde solution. The fixed tissues were dehydrated through a concentration gradient of ethanol (50%, 70%, 90% and 100% alcohol), embedded into the paraffin, sectioned at a thickness of 3–5 μm, mounted onto glass slides and stained with Haematoxylin & Eosin (HE). The villus width, villus height, crypt depth and images were observed with a Leica microsystems (CMS GmbH Ernst-Leitz-Str, Wetzlar, Germany).

Quantitative real-time PCR (qRT-PCR)

Jejunum mucosa was sampled by using sterile glass slides, put to liquid nitrogen quickly and then transferred to -80°C freezer. Total RNA was extracted using Steadypure Universal RNA Extraction Kit (Accurate Biology, China, AG21017). After examination of RNA purity and quality, reverse transcription was conducted with EVO M-MLV RT premix for qPCR (Accurate Biology, China, AG11706-S) in T100 Thermal Cycler (Bio-Rad, Singapore, 621BR47201). The quantification of the gene was carried out by SYBR Green Pro Taq HS qPCR Kit (Accurate Biology, China, AG11701), three duplicates per sample. The total reaction mixture of 20 μl contained the following: 10 μl of 2×SYBR Green Pro Taq HS premix (Accurate Biology), 0.4 μl of each primer (primers sequence seen at Table 1), 1 μl of cDNA and 8.2 μl of RNase free water. The qPCR reaction procedure parameters: 95°C for 30 s, 40 cycles of 95°C for 5 s, and 60°C for 30 s. The mRNA expression was calculated by the method of the $2^{-\Delta\Delta Ct}$ and presented as the fold change compared to the control group.

Table 2
Primer nucleotide sequences and information

Gene name	Primers sequence (5' to 3')	GenBank Accession
TNF-α	F: CTCCACTTGCGGGTTTGCTAC	NM_001082263.1
	R: AAGAGTCCCCAAACAACCTCC	
IL-6	F: GCCCATGAAATTCCGCAAG	NM_001082064.2
	R: GAAGACGACCACGATCCAC	
IL-1 β	F: AGACTCAAATTCCAGCTTGTCC	NM_001082201.1
	R: AAGACGATAAACCTACCCTGC	
GAPDH	F: TTCCCGTTCTCAGCCTTGACC	NM_001082253.1
	R: TGCTGATGAGTACAACCGACT	
NOS2	F: GCATCTTGGAACGAGTAGTGGACTG	XM_017349094.1
	R: TAGGTGAGGGCTTGGCTGAGTG	
GRO-B	F: CATCCAGAACCTGAAGGTGCTGTC	XM_002717021.3
	R: AGTTGCCATTGCTGAGCCTCTTC	
ICAM-1	F: TCTTGAACAGTGACAGCCCTT	AB128157.1
	R: TGCTCCGTGGGAATGAGAC	

The RNA Sequencing and Analysis

A total amount of 1 μg RNA per sample was used as input material for the RNA sample preparations. Sequencing libraries were generated using NEBNext UltraTM RNA Library Prep Kit for Illumina (NEB, USA) and index codes were added to attribute sequences to each sample. The raw reads were further processed with a bioinformatic pipeline tool, BMKCloud (www.biocloud.net) online platform.

Raw data (raw reads) of fastq format were firstly processed through in-house Perl scripts. In this step, clean data (clean reads) were obtained by removing adapter, ploy-N and low-quality reads from raw data. At the same time, Q20, Q30, GC-content and sequence duplication levels of the clean data were calculated. All the downstream analysis were based on clean data with high quality. Gene function was annotated based on the following databases: Nr (NCBI non-redundant protein sequences), Nt (NCBI non-redundant nucleotide sequences); Pfam (Protein family), KOG/COG (Clusters of Orthologous Groups of proteins), Swiss-Prot (A manually annotated and reviewed protein sequence database), KO (KEGG Ortholog database); GO (Gene Ontology).

UHPLC-QTOF-MS serum non-targeted metabolomics

LC-MS/MS analysis was performed using a UHPLC system (1290, Agilent Technologies) with a UPLC BEH Amide column (1.7μm, 2.1×100 mm, Waters) coupled to TripleTOF 5600 (Q-TOF, AB Sciex). The mobile phase consisted of 25mM NH_4OAc and 25mM NH_4OH in water (pH=9.75) (A) and acetonitrile (B) was carried with elution gradient as follows: 0 min, 95% B; 7 min, 65% B; 9 min, 40% B; 9.1 min, 95% B; 12 min, 95% B, which was delivered at 0.5 $mL{\cdot}min^{-1}$. The injection volume was 3 μL. The Triple TOF mass spectrometer was used to acquire MS/MS spectra on an information-dependent basis during an LC/MS experiment. In this mode, the acquisition software (Analyst TF 1.7, AB Sciex) continuously evaluates the full scan survey MS data as it collects and triggers the acquisition of MS/MS spectra depending on preselected criteria. In each cycle, 12 precursor ions with intensity greater than 100 were chosen for fragmentation at collision energy of 30 V (15 MS/MS events with a production accumulation time of 50 msec each). Electrospray ionization source conditions were as follows: Ion source gas 1 set for 60 Psi, Ion source gas 2 set for 60 Psi, Curtain gas set for 35 Psi, source temperature 650°C, Ion Spray Voltage Floating 5000 V or -4000 V in positive or negative modes, respectively.

KEGG pathway enrichment analysis

KEGG[40] is a database resource for understanding high-level functions and utilities of the biological system, such as the cell, organism and ecosystem, from molecular-level information, especially large-scale molecular datasets generated by genome sequencing and other high-throughput experimental technologies (http://www.genome.jp/kegg/). We used KOBAS[41] software to test the statistical enrichment of differential expression genes in KEGG pathways.

Weighted Gene Co-expression Network Analysis

The overlapping differentially expressed genes (DEG) and the overlapping serum glycerophospholipids in differential metabolites (DM) were selected for co-expression network analysis through the Weighted Gene Co-expression Network Analysis tool from Bioinfo Intelligent Cloud (www.ehbio.com). The content of an overlapping DM was used as a trait, and module plot, module gene trait correlation plot, etc. were obtained through WGCNA.

Statistical Analysis

Differential expression analysis of two conditions/groups were performed using the DESeq2 which provides statistical routines for determining differential expression in digital gene expression data using a model based on the negative binomial distribution. The resulting P values were adjusted by Benjamini and Hochberg's approach to

control the false discovery rate. Genes with an adjusted P < 0.01 found by DESeq2 were assigned as DEG. Metabolomic raw data files were converted to the mzXML format using ProteoWizard and processed by R package XCMS (version 3.2). The preprocessing results generated a data matrix consisted of the retention time (RT), mass-to-charge ratio (m/z) values and peak intensity. R package CAMERA was used for peak annotation after XCMS data processing. An in-house MS2 database was applied in metabolites identification. Metabolites with P < 0.05 were considered as DMs. The data of growth performance and real-time qPCR were processed by one-way ANOVA in SPSS 20.0 and Turkey test were used for Post Hoc Multiple comparisons. P < 0.05 were considered as significant difference. All the data presented as mean ± SEM.

Results

Serum metabolome and RNA-seq showed that I3C improved the growth performance of rabbits through enhancing nutrition digestion and absorption

In I3C supplemental assay, we detected growth performance in control group and I3C group. I3C decreased FCR (*P<0.05*), but exerted no significant influence (*P>0.05*) on AFDI and ADG (Fig. 1a), compared to control group. To explore how I3C improved growth performance, the RNA-seq was performed in the jejunum mucosa of rabbits. The plot from principal component analysis (PCA) of gene expression presented the significant difference between I3C and control group (Fig. 1b), and the KEGG enriched pathways revealed I3C activated protein digestion and absorption signaling pathway and the intestinal immune network signaling pathway for IgA production (Fig. 1d). To confirm the results of RNA-seq, serum metabolome analysis was conducted. The orthogonal partial least squares discriminant analysis (OPLS-DA) showed a marked separate trend on the serum metabolites of two groups (Fig. 1c), and the serum metabolomic KEGG enriched pathways showed that the digestion and absorption pathway of protein, vitamin, lipid, especially biosynthesis of amino acids pathway were activated in I vs. C (Fig. 1e).

I3C modulated a broad range of signaling pathways related to metabolism and inflammation

RNA-seq results showed the most DEGs enriched in human diseases signaling pathway, environment information processing pathway and metabolism pathway in C vs. L (Fig. 2a). However, we found the most DEGs enriched in metabolism and human diseases in L vs. IL (Fig. 2b). There were 1250 genes increased and 1385 genes diminished significantly by LPS group compared to control group; 237 genes were increased and 121 genes were decreased significantly by I3C+LPS group compared to LPS group (Fig. 2c, Fig. 2d, Supplementary Table 1). From the heatmap of three groups, we found control group exert no significant separation with the I3C+LPS group, compared to the LPS group (Fig. 2e). Among the overlapping pathways in the comparison of the down-regulated KEGG enriched pathways in C vs. L (Fig. 2f) with the up-regulated KEGG enriched pathways in L vs. IL (Fig. 2g), metabolism of xenobiotics by cytochrome P450, drug metabolism-cytochrome P450 and drug metabolism-other enzymes belonged to xenobiotics biodegradation and metabolism signaling pathway; steroid biosynthesis and steroid hormone biosynthesis belonged to lipid metabolism signaling pathway; glycolysis/gluconeogenesis, ascorbate and aldarate metabolism, pentose and glucuronate interconversions belonged to carbohydrate metabolism signaling pathway; folate biosynthesis, porphyrin and chlorophyll metabolism and retinol metabolism belonged to the metabolism of cofactors and vitamins signaling pathways. Peroxisome and PPAR signaling pathways related to lipid transport and metabolism, glucose metabolism and immune response. We also noted I3C had activated the chemical carcinogenesis signaling pathway which was justly activated by the expression of the I3C decomposition protein (cytochrome P450), with no carcinogenesis effect.

Further analysis of the correlation network plot (Fig. 2h) revealed pentose and glucuronate interconversions, and ascorbate and aldarate metabolism were correlated with cytochrome P450 activated by I3C. KEGG enriched pathways mining showed PPAR signaling pathway might mediate the anti-inflammatory effect by I3C. I3C activated the expression of the upstream and downstream gene of PPARs, such as SCD, CYP27A1, MEI, APOC3, FABP1, PCK2, ACSL1, ANGPTL4, SLC27A4, HAMGCS2. (Fig. 2i).

I3C alleviated LPS-induced intestinal inflammation and injury

I3C inhibited the expression of pro-inflammatory cytokines (TNF-α, IL-6, IL-1β, ICAM1, NOS2) upregulated by LPS in Fig. 3a (*P<0.05*). According to histological analysis of jejunum tissues, the obvious intestinal injury occurred in the LPS group, such as thinner mucosa, more swelled villus than that in other groups (Fig. 3b). The villus height of LPS and I3C+LPS group was significantly decreased (*P<0.05*), compared to control group. However, there was no difference in villus width, crypt depth and V/C among all the groups (*P>0.05*, Fig. 3c).

I3C restored the changes of serum metabolites and signaling pathways disturbed by LPS

The serum metabolites differences between the LPS and control group (Fig. 4a) were obvious, as well in the LPS and I3C+LPS group (Fig. 4b). There are 1975 and 276 DMs in C vs. L and L vs. IL respectively, with 146 overlapping DMs (Supplementary Fig. 1a). According to the classification annotation information of the Human Metabolome Database (HMDB), most DMs were mainly attributed to carboxylic acids and derivatives, glycerophospholipids, steroids and steroid derivatives, fatty acyls, prenol lipids and organooxygen compounds in the comparison of C vs. L (Supplementary Fig. 1b) and L vs. IL (Supplementary Fig. 1c). The heatmap showed control group has no significant difference from the I3C+LPS group (Fig. 4c). Moreover, the comparison of the KEGG enriched pathway in C vs. L (Fig. 4d) and L vs. IL (Fig. 4e) indicated glycerophospholipid metabolism and choline metabolism in the cancer signaling pathway were the most enriched overlapping pathway. Additionally, the serum metabolites in choline metabolism pathway were correlated with glycerophospholipid metabolism pathway (Fig. 4f, Fig. 4g), then we further carry our research from glycerophospholipid.

The serum concentrations of PE (24:0/24:1(15Z)), PE (14:1(9Z)/20:5(5Z,8Z,11Z,14Z,17Z)), PE (20:2(11Z,14Z)/24:0), PC (16:0/24:1(15Z)), PC (o-22:0/18:3(6Z,9Z,12Z)), PC (o-22:0/18:3(6Z,9Z,12Z)) and PC (16:0/24:1(15Z)) in LPS group were decreased significantly compared to control group (*P<0.01*), while the concentration of PE (20:2(11Z,14Z)/16:0), PC (16:0/20:4(8Z,11Z,14Z,17Z)) and PC (20:2(11Z,14Z)/14:0) in LPS group were higher significantly (*P<0.01*) than control group, which were reversed by I3C (Table 3).

Table 3 The differential glycerophospholipids in serum.

Item	Metabolite name	C vs. L			L vs. IL		
		log_2FC	P value	regulated	log_2FC	P value	regulated
1	PE (24:0/24:1(15Z))	-1.44	0.0003	down	1.47	0.0034	up
2	PE (14:1(9Z)/20:5(5Z,8Z,11Z,14Z,17Z))	-1.21	0.0002	down	0.75	0.0007	up
3	PE (20:2(11Z,14Z)/24:0)	-1.29	0.0012	down	1.44	0.0009	up
4	PC (16:0/24:1(15Z))	-1.17	0.0016	down	0.66	0.0032	up
5	PC (o-22:0/18:3(6Z,9Z,12Z))	-0.85	0.0001	down	0.73	0.0003	up
6	PE (20:2(11Z,14Z)/16:0)	0.79	0.0018	up	-0.13	0.0445	down
7	PC (16:0/20:4(8Z,11Z,14Z,17Z))	1.25	0.0006	up	-0.13	0.0178	down
8	PC (20:2(11Z,14Z)/14:0)	2.06	0.0002	up	-0.08	0.0474	down

Fold change was calculated based on normalized peak intensities in LPS group (L) divided by those in healthy control rabbit (C) or those in I3C+LPS group (IL) divided by L.

The combined analysis of serum glycerophospholipids with RNA-seq

To investigate the effect of glycerophospholipid, WGCNA was conducted using FPKM values of the overlapping DEGs (Supplementary Table 2) and DMs (Table 3). Traits 1-8 in the WGCNA maps corresponded to the order of metabolites in Table 3. The plot of WGCNA module trait correlation showed the DEGs were identified into four modules: blue module (MEblue), brown module (MEbrown), grey module (MEgrey) and turquoise module (MEturquoise) (Fig. 5a). MEblue and MEturquoise exhibited a high positive correlation with each other, while MEbrown showed low correlation with them (Fig. 5b). From Network visualization of WGCNA hub genes, the MEblue and MEturquoise can be attributed to metabolism, and MEbrown mainly related to immunity (Fig. 5c). Additionally, Trait 1, Trait 2, Trait 3, Trait 4, and Trait 5 regulated metabolic and inflammatory related genes positively, especially metabolic genes, contrary to Trait 6, Trait 7, and Trait 8 (Fig. 5d). Among these glycerophospholipids, PE(20:2(11Z,14Z)/24:0), PC (16:0/24:1(15Z)), PE(20:2(11Z,14Z)/16:0), PC(16:0/20:4(8Z,11Z,14Z,17Z)), PC (20:2(11Z,14Z)/14:0) were correlated with intestinal immunity significantly. From analysis of Pearson's correlation, we found PC (16:0/24:1(15Z))) and (PC (20:2(11Z,14Z)/14:0)) participated in immunity regulatory network which consisted of JAK2, NOS2, RIPK2, ICAM1, GRO-B, TMEM173, ME1, FABP1 and APOC3 (Supplemental Table 3 and Supplemental Table 4). The specific regulatory relationship was shown in Fig 5e. The grey module showed very low correlation with other modules and traits, and had little research value, therefore it was ignored.

Discussion

I3C has good curative effects on autoimmune encephalomyelitis [42], carbon tetrachloride-induced liver injury [43], doxorubicin-induced genotoxicity and cardiotoxicity [28], chicken coccidiosis [21] and so on, through alleviating inflammation and oxidative stress. Most research of I3C on intestinal inflammation focused on colitis [44–47], while little research fixed attention to enteritis associated with high mortality in animal production. Our study revealed I3C improved growth performance by decreasing FCR. From the KEGG enriched pathways of the RNA-seq and serum

metabolome, we knew I3C increased growth performance mainly by activating protein digestion and absorption signaling pathway. In the study I3C decreased the expression of IgA, which was upregulated by LPS (Supplementary Table2). Intestinal IgA is regulated by AhR, in which endogenous and exogenous ligands could promote the production of IgA [48], but according to Yoshida's study, 2-(1'H-indole-3'-carbonyl)-thiazole-4-carboxylic acid methyl ester, the high affinity ligand of AhR, suppressed the expression of IgM, IgE and IgG1 in purified mouse B cells stimulated with anti-CD40 antibody and interleukin-4 [49]. Therefore, we speculated I3C regulated the differentiation and expression of B cells by promoting the production of IgA to maintain intestinal homeostasis in health and suppressing the expression of IgA under inflammation to reduce intestinal injury.

In the comparison of I3C + LPS and LPS group, I3C recovered lipid, carbohydrate, cofactors and vitamins metabolism as serum metabolome and RNA-seq shown. LPS suppressed the expression of cytochrome P450, which was reversed by I3C. In the correlation network plot of RNA-seq, we found pentose and glucuronate interconversions pathway, and ascorbate and aldarate metabolism pathway correlated with cytochrome P450 significantly. Cytochrome P450 regulated the metabolism of the endogenous compounds such as steroid, vitamins, etc., and exogenous compounds[50]. However, there is no report about the relationship between cytochrome P450 and pentose and glucuronate interconversions signaling pathway. In our study, cytochrome P450 signaling pathway (drug metabolism-cytochrome P450, metabolism of xenobiotics by cytochrome P450 and chemical carcinogenesis signaling pathway) and pentose and glucuronate interconversions signaling pathway shared the same DEGs such as UGT2B14, UGT2B13, UGT1 and UGT1A7, the subtypes of the gene encoding glucuronosyltransferase (Supplementary Table2). Glucuronosyltransferase is involved in the metabolism of 20% clinical drugs and downregulated under an inflammatory state [51], which is consistent with us that I3C alleviated the suppression of glucuronosyltransferase induced by LPS. As a result, we extrapolated that I3C improved the metabolic disorder of the small intestine induced by LPS through the expression alteration of cytochrome P450.

Histological analysis in Jejunum mucosa presented I3C alleviated the swelling effect of intestinal villus induced by LPS. However, I3C didn't alter villus width, villus height, crypt depth, and V/C. I3C showed no significant alteration to villus height and crypt depth in report [52], while had good effect of reducing inflammation response [22, 53]. In the study, I3C alleviated the release of pro-inflammatory cytokines (TNF-α, IL-6, iNOS, ICAM1, GRO-B) caused by LPS. We also found from the RNA-seq that I3C promoted the mRNA expression of intestinal alkaline phosphatase (Supplementary Table2) which participated in detoxifying LPS and attenuating LPS-induced intestinal inflammation [54]. Some blood metabolites could be the inflammatory markers reflecting intestinal injury [55], while the intestinal signaling pathway can regulate blood metabolites [56]. The combined analysis of the RNA-seq and serum metabolites showed glycerophospholipids were the main altered serum metabolites and might be inflammatory markers in this study. Some glycerophospholipids were detected to be biomarkers of Crohn's disease and ulcerative colitis [36], and low PC in intestinal epithelial cells were related to colonic barrier dysfunction [57]. Therefore, the WGCNA analysis was performed on glycerophospholipids with all DEGs. As results shown, PC (16:0/24:1(15Z)) was negatively regulated inflammatory response, while the anti-inflammatory effect of PC (16:0/24:1(15Z)) has seldom reports. The research pointed out that it decreased significantly in the serum of pregnancies with congenital heart defects [58]. However, PC (20:2(11Z,14Z)/14:0) was positively correlated with inflammatory pathways, in agreement with Cho [59]and Wahl [60] who found PC (20:2(11Z,14Z)/14:0) the marker of inflammation-related disorders in blood of obese people. Moreover, PC (20:2(11Z,14Z)/14:0) was upregulated in the lung, colorectal and gastric cancer, as a biomarker that differentiated different pathophysiological states or cancer stages [61]. In our study, I3C altered the imbalance of serum concentration of PC (16:0/20:4(8Z,11Z,14Z,17Z)) and PC (20:2(11Z,14Z)/14:0) induced by LPS (Table 3).

PPAR signaling pathways were overlapping pathway in C vs. L and L vs. IL, of which upstream and downstream structural genes (Fig. 2i and Supplementary Table2) were regulated significantly rather than transcription factors (PPARα, PPARγ, PPARβ/δ). PPARs suppressed the pro-inflammatory genes by preventing transcription factors like NF-κB, AP-1, C/EBP, STAT and NF-AT from binding to their DNA response elements [62], and participated in glucose, lipid metabolism and regulate energy homeostasis [63]. Cytochrome P450 1A1 (CYP1A1) and Cytochrome P450 1B1 (CYP1B1) both activated the expression of PPARs [64, 65], while I3C promoted the expression of CYP1A1 rather than CYP1B1 in this study (shown in Supplementary Table2). Therefore, the PPAR signaling pathway may be activated by CYP1A1 partly. Additionally, endogenous PCs generated from endogenous lipid can be the ligand for PPARα [66, 67]. In the present study, PC (16:0/24:1(15Z)) was found positively correlated with ME1, FABP1, APOC3 and negatively correlated with GRO-B, TMEM173, RIPK2, JAK2, ICAM1. Family members of FABP possess different lipid ligand-binding specificity and affinity, and could interact with different intracellular functional proteins including PPARs, among which FABP1 was predominantly expressed in the liver [68]. Combining our results with the previous reports, we get the anti-inflammatory mechanism of PC (16:0/24:1(15Z)) as follows: FABP was specifically bonded to PC (16:0/24:1(15Z)), and interacted with intracellular PPARs to upregulate the expression of Malic enzyme (ME1), Apolipoprotein CIII (APOC3), FABP1, etc. Meanwhile, PPARs inhibited the binding of NFkB and STAT to DNA response element region and weakened the mRNA expression of RIPK2, JAK2, GRO-B and ICAM1. From the PCCs of PC (20:2(11Z,14Z)/14:0) in immunity regulatory network, we thought it might be a specific inhibitor of PPARs, while related research was not noted until now. Despite these promising results, the question remains about how I3C regulated the serum concentrations of PC (16:0/24:1(15Z)) and PC (20:2(11Z,14Z)/14:0). A possible explanation for this might refer to the glycerophospholipid metabolism pathway. From RNA-seq data, we found SPLA2 which regulated the hydrolysis of PCs [69] in glycerophospholipid metabolism pathway negatively correlated with PC (16:0/24:1(15Z)) and activated by LPS [70], while I3C suppressed the expression of SPLA2 (Supplementary Table2). However, PC (20:2(11Z,14Z)/14:0) was not correlated with sPLA2 but SLC44A4 positively. The SLC44A4, encoded choline transporter, involved in phospholipid synthesis [71], was decreased by I3C in the treatment of LPS in jejunum (Supplementary Table2). No reports could show the specific way of I3C regulating PC (20:2(11Z,14Z)/14:0) clearly. The reason that the I3C can alleviated inflammation and metabolic disorder induced by LPS through PPAR pathways may be either CYP1A1-dependent activation or PC (16:0/24:1(15Z))-dependent activation. I3C regulated the PC (16:0/24:1(15Z)) though improving the biosynthesis and metabolism of PCs.

Conclusion

In summary, I3C can improve growth performance through enhancing nutrition digestion and absorption, and increase intestinal immunity. I3C suppressed the activation of intestinal inflammatory pathways and metabolic disorder induced by LPS through activating the PPAR signaling pathway by CYP1A1, and may also be involved in anti-inflammatory effects by improving glycerophospholipids synthesis and metabolism. Moreover, we found PC (16:0/24:1(15Z)) may be a endogenous ligand of PPAR, and PC (20:2(11Z,14Z)/14:0) was a potential inflammatory biomarker.

Abbreviations

I3C: Indole-3-carbinol; ITE: 2-(1'H-indole-3'-carbonyl)-thiazole-4-carboxylic acid methyl ester; AhR: Aryl hydrocarbon receptor; ETEC: enterotoxigenic Escherichia coli; TNF-α: Tumour necrosis factor α; IL-6: Interleukin-6; IL-1β: Interleukin-1β; ICAM1: intercellular adhesion molecule 1; NOS2:nitric-oxide synthase; GRO-B: GRO beta protein or C-X-C motif chemokine 1/2/3; LPS: Lipopolysaccharide; ADG: Average daily gain; ADFI: Average daily feed intake;

FCR: Feed conversion ratio; PPAR: Peroxisome proliferator-activated receptors; ME1: Malic enzyme; APOC3 Apolipoprotein CIII; FABP: Fatty acid binding protein; qRT-PCR: Quantitative real-time PCR; IAP: alkaline phosphatase; PE: Phosphatidylethanolamines; PC: phosphatidylcholine; RIPK2: receptor-interacting serine/threonine-protein kinase 2; CYP1A1: Cytochrome P450 1A1; CYP1B1: Cytochrome P450 1B1; JAK2: Janus kinase 2; sPLA2: secreted phospholipase 2 (sPLA2); SLC44A4: solute carrier family 44 member 4.

Declarations

Acknowledgments

The authors thank BMKCloud (Beijing) for providing the assay work for RNA-seq and serum metabolites, and data analysis platform. The authors also thank Juncai Chen, the associate professor of College of Animal Science and Technology, Southwest University, Beibei, Chongqing, China, for giving some guidance.

Authors' contributions

Zihan Guo and Jingzhi Lu designed the study; Zihan Guo mainly wrote and revised the manuscript; Jingzhi Lu reviewed the manuscript; Zihan Guo, Na Zhao, and Jingzhi Lu conducted the experiments and determination of parameters; Zihan Guo, Na Zhao, Jingzhi Lu, Wangcheng Liu, Puran Chen, Xiang Fu, Bin Wang, Xin Ye, and Jing Li contributed to animal feeding, and data analyses were conducted by Zihan Guo, Na Zhao, Jingzhi Lu. All authors read and approved the final manuscript.

Funding

This study was supported by the Special general project for technological innovation and application development of Chongqing Science and Technology Bureau (cstc2020jscx-msxmX0049), and Chongqing modern mountain characteristic high-efficiency agricultural industrial technology system (Herbivorous livestock 2020 [11]).

Availability of data and materials

Most data for this article are included within the article and additional files, and the rest data can be obtained from the corresponding author on request.

Ethics approval and consent to participate

Experimental procedures and animal use were approved by the Ethics Committee of animal welfare at Southwest University (IACUC Issue No. 20210122-1).

Consent for publication

Not applicable.

Competing interests

The authors declare that they have no conflict of interest.

References

[1] NOSRATABABADI R, BAGHERI V, ZARE-BIDAKI M, et al. Toll like receptor 4: an important molecule in recognition and induction of appropriate immune responses against Chlamydia infection [J]. Comparative Immunology Microbiology and Infectious Diseases, 2017, 51: 27-33.

[2] WANG X, QUINN P J. Endotoxins: Lipopolysaccharides of Gram-Negative Bacteria [M]. Endotoxins: Structure, Function and Recognition. Dordrecht; Springer Netherlands. 2010: 3-25.

[3] TANG J, XU L Q, ZENG Y W, et al. Effect of gut microbiota on LPS-induced acute lung injury by regulating the TLR4/NF-kB signaling pathway [J]. International Immunopharmacology, 2021, 91.

[4] GUO S H, NIGHOT M, AL-SADI R, et al. Lipopolysaccharide Regulation of Intestinal Tight Junction Permeability Is Mediated by TLR4 Signal Transduction Pathway Activation of FAK and MyD88 [J]. Journal of Immunology, 2015, 195(10): 4999-5010.

[5] PEREZ-HERNANDEZ E G, DELGADO-COELLO B, LUNA-REYES I, et al. New insights into lipopolysaccharide inactivation mechanisms in sepsis [J]. Biomedicine & pharmacotherapy = Biomedecine & pharmacotherapie, 2021, 141: 111890.

[6] GORDON J I. Honor Thy Gut Symbionts Redux [J]. Science, 2012, 336(6086): 1251-1253.

[7] AGUS A, PLANCHAIS J, SOKOL H. Gut Microbiota Regulation of Tryptophan Metabolism in Health and Disease [J]. Cell Host & Microbe, 2018, 23(6): 716-724.

[8] CHEN F D, WU W, CONG Y Z. Short chain fatty acids regulation of neutrophil production of IL-10 [J]. Journal of Immunology, 2016, 196.

[9] KANG J D, MYERS C J, HARRIS S C, et al. Bile Acid 7 alpha-Dehydroxylating Gut Bacteria Secrete Antibiotics that Inhibit Clostridium difficile: Role of Secondary Bile Acids [J]. Cell Chemical Biology, 2019, 26(1): 27-+.

[10] ROMANI L, ZELANTE T, DE LUCA A, et al. Microbiota control of a tryptophan-AhR pathway in disease tolerance to fungi [J]. European Journal of Immunology, 2014, 44(11): 3192-3200.

[11] ATREYA R, NEURATH M F. Molecular pathways controlling barrier function in IBD [J]. Nature Reviews Gastroenterology & Hepatology, 2015, 12(2): 67-68.

[12] SCALDAFERRI F, PIZZOFERRATO M, PECERE S, et al. Bacterial Flora as a Cause or Treatment of Chronic Diarrhea [J]. Gastroenterology Clinics of North America, 2012, 41(3): 581-+.

[13] VARGAS-CARAVEO A, SAYD A, MAUS S R, et al. Lipopolysaccharide enters the rat brain by a lipoprotein-mediated transport mechanism in physiological conditions [J]. Scientific Reports, 2017, 7.

[14] YARLAGADDA A, ALFSON E, CLAYTON A H. The blood brain barrier and the role of cytokines in neuropsychiatry [J]. Psychiatry (Edgmont), 2009, 6(11): 18-22.

[15] SOARES R L S. Irritable bowel syndrome: A clinical review [J]. World Journal of Gastroenterology, 2014, 20(34): 12144-12160.

[16] LUCAS M, CHOCANO-BEDOYA P, SCHULZE M B, et al. Inflammatory dietary pattern and risk of depression among women [J]. Brain Behav Immun, 2014, 36: 46-53.

[17] QADRI F, SVENNERHOLM A M, FARUQUE A S, et al. Enterotoxigenic Escherichia coli in developing countries: epidemiology, microbiology, clinical features, treatment, and prevention [J]. Clin Microbiol Rev, 2005, 18(3): 465-483.

[18] FAIRBROTHER J M, NADEAU E, GYLES C L. Escherichia coli in postweaning diarrhea in pigs: an update on bacterial types, pathogenesis, and prevention strategies [J]. Animal Health Research Reviews, 2005, 6(1): 17-39.

[19] BAKO E, KAGAMBEGA A, TRAORE K A, et al. Characterization of Diarrheagenic Escherichia coli Isolated in Organic Waste Products (Cattle Fecal Matter, Manure and, Slurry) from Cattle's Markets in Ouagadougou, Burkina Faso [J]. International Journal of Environmental Research and Public Health, 2017, 14(10).

[20] VAN BOECKEL T P, BROWER C, GILBERT M, et al. Global trends in antimicrobial use in food animals [J]. Proc Natl Acad Sci U S A, 2015, 112(18): 5649-5654.

[21] KIM W H, LILLEHOJ H S, MIN W. Indole Treatment Alleviates Intestinal Tissue Damage Induced by Chicken Coccidiosis Through Activation of the Aryl Hydrocarbon Receptor [J]. Frontiers in Immunology, 2019, 10.

[22] WU Y B, HE Q, YU L L, et al. Indole-3-Carbinol Inhibits Citrobacter rodentium Infection through Multiple Pathways Including Reduction of Bacterial Adhesion and Enhancement of Cytotoxic T Cell Activity [J]. Nutrients, 2020, 12(4).

[23] MEZRICH J D, FECHNER J H, ZHANG X J, et al. An Interaction between Kynurenine and the Aryl Hydrocarbon Receptor Can Generate Regulatory T Cells [J]. Journal of Immunology, 2010, 185(6): 3190-3198.

[24] VELDHOEN M, HIROTA K, CHRISTENSEN J, et al. Natural agonists for aryl hydrocarbon receptor in culture medium are essential for optimal differentiation of Th17 T cells [J]. Journal of Experimental Medicine, 2009, 206(1): 43-49.

[25] KADO S, CHANG W L W, CHI A N, et al. Aryl hydrocarbon receptor signaling modifies Toll-like receptor-regulated responses in human dendritic cells (vol 91, pg 2209, 2017) [J]. Archives of Toxicology, 2017, 91(7): 2713-2713.

[26] SONG J M, QIAN X, MOLLA K, et al. Combinations of indole-3-carbinol and silibinin suppress inflammation-driven mouse lung tumorigenesis by modulating critical cell cycle regulators [J]. Carcinogenesis, 2015, 36(6): 666-675.

[27] WU Y B, LI R W, HUANG H Q, et al. Inhibition of Tumor Growth by Dietary Indole-3-Carbinol in a Prostate Cancer Xenograft Model May Be Associated with Disrupted Gut Microbial Interactions [J]. Nutrients, 2019, 11(2).

[28] HAJRA S, PATRA A R, BASU A, et al. Prevention of doxorubicin (DOX)-induced genotoxicity and cardiotoxicity: Effect of plant derived small molecule indole-3-carbinol (I3C) on oxidative stress and inflammation [J]. Biomedicine & Pharmacotherapy, 2018, 101: 228-243.

[29] CHOI Y, KIM Y, PARK S, et al. Indole-3-carbinol prevents diet-induced obesity through modulation of multiple genes related to adipogenesis, thermogenesis or inflammation in the visceral adipose tissue of mice [J]. Journal of Nutritional Biochemistry, 2012, 23(12): 1732-1739.

[30] AHN M, KIM J, YANG D, et al. Indole-3-carbinol alleviates carbon tetrachloride-induced liver injury by inhibiting inflammatory response and regulating lipid metabolism [J]. Advances in Traditional Medicine, 2021,

21(2): 371-378.

[31] FAHY E, SUBRAMANIAM S, BROWN H A, et al. A comprehensive classification system for lipids [J]. Journal of Lipid Research, 2005, 46(5): 839-861.

[32] ASTUDILLO A M, BALGOMA D, BALBOA M A, et al. Dynamics of arachidonic acid mobilization by inflammatory cells [J]. Biochimica Et Biophysica Acta-Molecular and Cell Biology of Lipids, 2012, 1821(2): 249-256.

[33] SCHMIDT J A, FENSOM G K, RINALDI S, et al. Pre-diagnostic metabolite concentrations and prostate cancer risk in 1077 cases and 1077 matched controls in the European Prospective Investigation into Cancer and Nutrition [J]. Bmc Medicine, 2017, 15.

[34] CHEN S, LIU C C. Ether Glycerophospholipids and Their Potential as Therapeutic Agents [J]. Current Organic Chemistry, 2013, 17(8): 802-811.

[35] LOPEZ-HERNANDEZ Y, LARA-RAMIREZ E E, SALGADO-BUSTAMANTE M, et al. Glycerophospholipid Metabolism Alterations in Patients with Type 2 Diabetes Mellitus and Tuberculosis Comorbidity [J]. Archives of Medical Research, 2019, 50(2): 71-78.

[36] MURGIA A, HINZ C, LIGGI S, et al. Italian cohort of patients affected by inflammatory bowel disease is characterised by variation in glycerophospholipid, free fatty acids and amino acid levels [J]. Metabolomics, 2018, 14(10).

[37] WU X, ZHAO L L, PENG H B, et al. Search for Potential Biomarkers by UPLC/Q-TOF-MS Analysis of Dynamic Changes of Glycerophospholipid Constituents of RAW264.7 Cells Treated With NSAID [J]. Chromatographia, 2015, 78(3-4): 211-220.

[38] CIFKOVA E, HOLCAPEK M, LISA M, et al. Determination of lipidomic differences between human breast cancer and surrounding normal tissues using HILIC-HPLC/ESI-MS and multivariate data analysis [J]. Analytical and Bioanalytical Chemistry, 2015, 407(3): 991-1002.

[39] ZHANG G, ZHAO L, ZHU J, et al. Anti-inflammatory activities and glycerophospholipids metabolism in KLA-stimulated RAW 264.7 macrophage cells by diarylheptanoids from the rhizomes of Alpinia officinarum [J]. Biomedical chromatography : BMC, 2018, 32(2).

[40] KANEHISA M, ARAKI M, GOTO S, et al. KEGG for linking genomes to life and the environment [J]. Nucleic Acids Research, 2008, 36: D480-D484.

[41] MAO X Z, CAI T, OLYARCHUK J G, et al. Automated genome annotation and pathway identification using the KEGG Orthology (KO) as a controlled vocabulary [J]. Bioinformatics, 2005, 21(19): 3787-3793.

[42] ROUSE M, SINGH N P, NAGARKATTI P S, et al. Indoles mitigate the development of experimental autoimmune encephalomyelitis by induction of reciprocal differentiation of regulatory T cells and Th17 cells [J]. British Journal of Pharmacology, 2013, 169(6): 1305-1321.

[43] AHN M, KIM J, YANG D, et al. Indole-3-carbinol alleviates carbon tetrachloride-induced liver injury by inhibiting inflammatory response and regulating lipid metabolism [J]. Advances in Traditional Medicine, 2021, 21(2): 371-378.

[44] ALKARKOUSHI R R, HUI Y N, TAVAKOLI A S, et al. Immune and microRNA responses toHelicobacter muridaruminfection and indole-3-carbinol during colitis [J]. World Journal of Gastroenterology, 2020, 26(32): 4763-4785.

[45] ALA M. Tryptophan metabolites modulate inflammatory bowel disease and colorectal cancer by affecting immune system [J]. International Reviews of Immunology, 2021.

[46] MEGNA B W, CARNEY P R, KENNEDY G D. Intestinal inflammation and the diet: Is food friend or foe? [J]. World Journal of Gastrointestinal Surgery, 2016, 8(2): 115-123.

[47] RIEMSCHNEIDER S, HOFFMANN M, SLANINA U, et al. Indol-3-Carbinol and Quercetin Ameliorate Chronic DSS-Induced Colitis in C57BL/6 Mice by AhR-Mediated Anti-Inflammatory Mechanisms [J]. International Journal of Environmental Research and Public Health, 2021, 18(5).

[48] CULBREATH C, TANNER S M, YERAMILLI V A, et al. Environmental-mediated intestinal homeostasis in neonatal mice [J]. Journal of Surgical Research, 2015, 198(2): 494-501.

[49] YOSHIDA T, KATSUYA K, OKA T, et al. Effects of AhR ligands on the production of immunoglobulins in purified mouse B cells [J]. Biomedical Research-Tokyo, 2012, 33(2): 67-74.

[50] GUENGERICH F P. Intersection of the Roles of Cytochrome P450 Enzymes with Xenobiotic and Endogenous Substrates: Relevance to Toxicity and Drug Interactions [J]. Chemical Research in Toxicology, 2017, 30(1): 2-12.

[51] FUJIWARA R, YODA E, TUKEY R H. Species differences in drug glucuronidation: Humanized UDP-glucuronosyltransferase 1 mice and their application for predicting drug glucuronidation and drug-induced toxicity in humans [J]. Drug Metabolism and Pharmacokinetics, 2018, 33(1): 9-16.

[52] PARK J H, LEE J M, LEE E J, et al. Indole-3-Carbinol Promotes Goblet-Cell Differentiation Regulating Wnt and Notch Signaling Pathways AhR-Dependently [J]. Molecules and Cells, 2018, 41(4): 290-300.

[53] JIANG J, KANG T B, SHIM D W, et al. Indole-3-carbinol inhibits LPS-induced inflammatory response by blocking TRIF-dependent signaling pathway in macrophages [J]. Food and Chemical Toxicology, 2013, 57: 256-261.

[54] MELO A D B, SILVEIRA H, BORTOLUZZI C, et al. Intestinal alkaline phosphatase and sodium butyrate may be beneficial in attenuating LPS-induced intestinal inflammation [J]. Genetics and Molecular Research, 2016, 15(4).

[55] SAITOH W, TAKADA S, HIRAO J, et al. Plasma citrulline is a sensitive safety biomarker for small intestinal injury in rats [J]. Toxicology Letters, 2018, 295: 416-423.

[56] SUN R, KONG B, YANG N, et al. The Hypoglycemic Effect of Berberine and Berberrubine Involves Modulation of Intestinal Farnesoid X Receptor Signaling Pathway and Inhibition of Hepatic Gluconeogenesis [J]. Drug Metabolism and Disposition, 2021, 49(3): 276-286.

[57] KENNELLY J P, CARLIN S, JU T T, et al. Intestinal Phospholipid Disequilibrium Initiates an ER Stress Response That Drives Goblet Cell Necroptosis and Spontaneous Colitis in Mice [J]. Cellular and Molecular Gastroenterology and Hepatology, 2021, 11(4): 999-1021.

[58] BAHADO-SINGH R O, ERTL R, MANDAL R, et al. Metabolomic prediction of fetal congenital heart defect in the first trimester [J]. American Journal of Obstetrics and Gynecology, 2014, 211(3).

[59] CHO K, MOON J S, KANG J H, et al. Combined untargeted and targeted metabolomic profiling reveals urinary biomarkers for discriminating obese from normal-weight adolescents [J]. Pediatric Obesity, 2017, 12(2): 93-101.

[60] WAHL S, HOLZAPFEL C, YU Z H, et al. Metabolomics reveals determinants of weight loss during lifestyle intervention in obese children [J]. Metabolomics, 2013, 9(6): 1157-1167.

[61] GUO Y, REN J, LI X, et al. Simultaneous Quantification of Serum Multi-Phospholipids as Potential Biomarkers for Differentiating Different Pathophysiological states of lung, stomach, intestine, and pancreas [J]. Journal of Cancer, 2017, 8(12): 2191-2204.

[62] RICOTE M, GLASS C K. PPARs and molecular mechanisms of transrepression [J]. Biochimica Et Biophysica Acta-Molecular and Cell Biology of Lipids, 2007, 1771(8): 926-935.

[63] HAN L, SHEN W J, BITTNER S, et al. PPARs: regulators of metabolism and as therapeutic targets in cardiovascular disease. Part II: PPAR-ss/delta and PPAR-gamma [J]. Future Cardiology, 2017, 13(3).

[64] FANG X M, ZHAO W M, XU J, et al. CYP1A1 mediates the suppression of major inflammatory cytokines in pulmonary alveolar macrophage (PAM) cell lines caused by Mycoplasma hyponeumoniae [J]. Developmental and Comparative Immunology, 2016, 65: 132-138.

[65] LARSEN M C, BUSHKOFSKY J R, GORMAN T, et al. Cytochrome P450 1B1: An unexpected modulator of liver fatty acid homeostasis [J]. Archives of Biochemistry and Biophysics, 2015, 571: 21-39.

[66] LAMAZIERE A, WOLF C. Phosphatidylcholine and PPAR alpha: A relevant connection in liver disease? [J]. Gastroenterologie Clinique Et Biologique, 2010, 34(4-5): 250-251.

[67] CHAKRAVARTHY M V, LODHI I J, YIN L, et al. Identification of a Physiologically Relevant Endogenous Ligand for PPAR alpha in Liver [J]. Cell, 2009, 138(3): 476-488.

[68] LI B, HAO J Q, ZENG J, et al. SnapShot: FABP Functions [J]. Cell, 2020, 182(4): 1066-+.

[69] HITE R D, SEEDS M C, JACINTO R B, et al. Hydrolysis of surfactant-associated phosphatidylcholine by mammalian secretory phospholipases A2 [J]. American journal of physiology Lung cellular and molecular physiology, 1998, 275(4): L740-L747.

[70] CAI T Q, THIEBLEMONT N, WONG B M, et al. Enhancement of leukocyte response to lipopolysaccharide by secretory group IIA phospholipase A(2) [J]. Journal of Leukocyte Biology, 1999, 65(6): 750-756.

[71] TRAIFFORT E, O'REGAN S, RUAT M. The choline transporter-like family SLC44: Properties and roles in human diseases [J]. Molecular Aspects of Medicine, 2013, 34(2-3): 646-654.

Figures

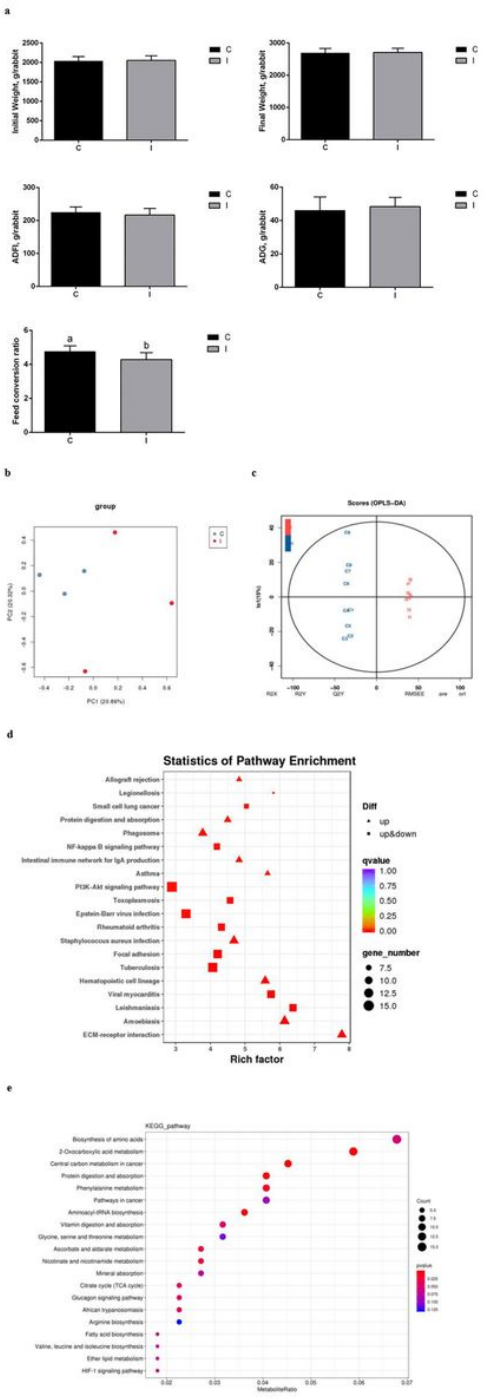

Figure 1

Exhibiting I3C effects on growth performance of rabbits in RNA-seq of jejunum mucosa and serum metabolome manner. Growth performance on experimental day 7 to day 21, including average daily weight gain (ADG), average daily feed intake (ADFI), feed conversion ratio (FCR). b PCA of DMs in C vs. I. c OPLS-DA of rabbit serum metabolites in the C vs. I. d KEGG enriched pathways of DEGs in C vs. I. e KEGG enriched pathway of DMs in C vs. I. C: control group; I: I3C group; L: LPS group; IL: I3C+LPS group. Different superscript letters (a, b) within the same picture mean differ significantly ($P < 0.05$).

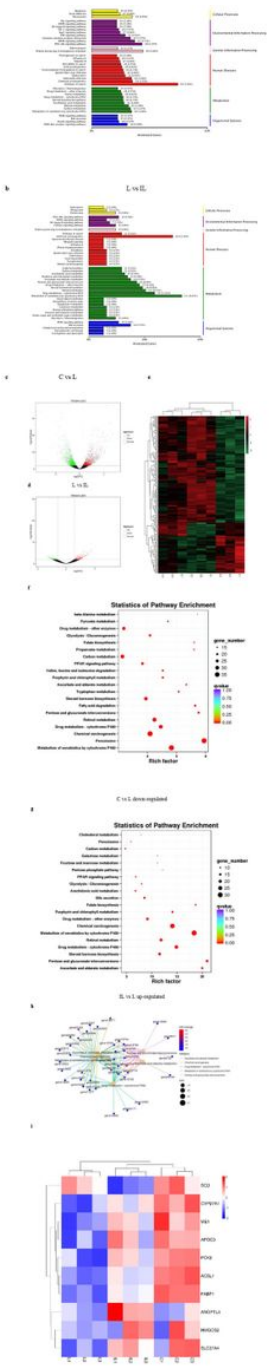

Figure 2

RNA-seq shows the gene expression in KEGG analysis way. a DEGs of the C vs. L classed in KEGG. b DEGs of L vs. IL classed in KEGG. c DEGs of control groups and LPS groups in Volcano plot map. Red spots indicate up-regulated genes and green spots indicate down-regulated genes. e The heatmap analysis of overlapping DEGs of Control, LPS, I3C+LPS group. f KEGG enriched pathways of down-regulated DEGs in L vs. C. g KEGG enriched pathways of up-regulated DEGs in IL vs. L. h Correlation network plot of KEGG enrich pathways in L vs. IL. i Cluster heat map of the PPAR signaling pathway. C: control group; I: I3C group; L: LPS group; IL: I3C+LPS group.

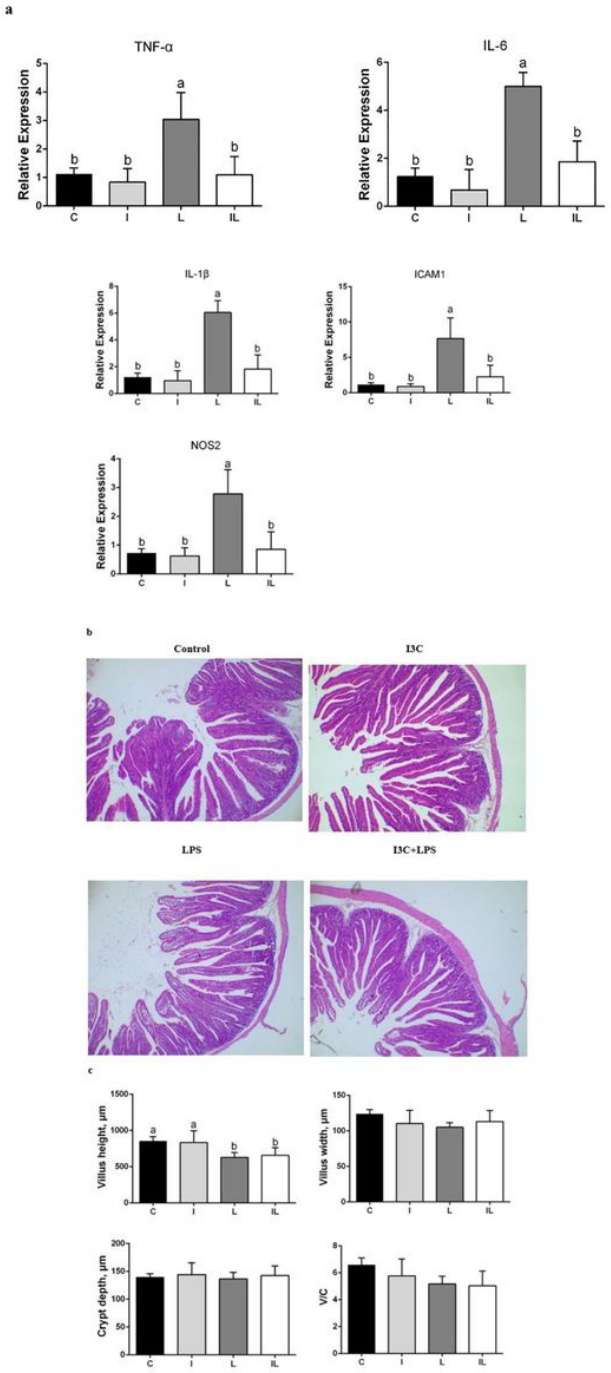

Figure 3

I3C attenuated LPS-induced intestinal inflammation, but didn' t change intestinal mucosal morphology. a The mRNA expression of pro-inflammatory genes in jejunum mucosa, including TNF-α, IL-6, IL-1β, ICAM1, and NOS2. b Picture display of hematoxylin and oil red-stained sections. c Intestinal morphology analysis, including villus height, villus width, crypt depth, and V/C in jejunum mucosa. All data were presented as mean ± SEM. Different superscript letters (a, b) within the same picture mean differ significantly ($P < 0.05$). C: control group; I: I3C group; L: LPS group; IL: I3C+LPS group.

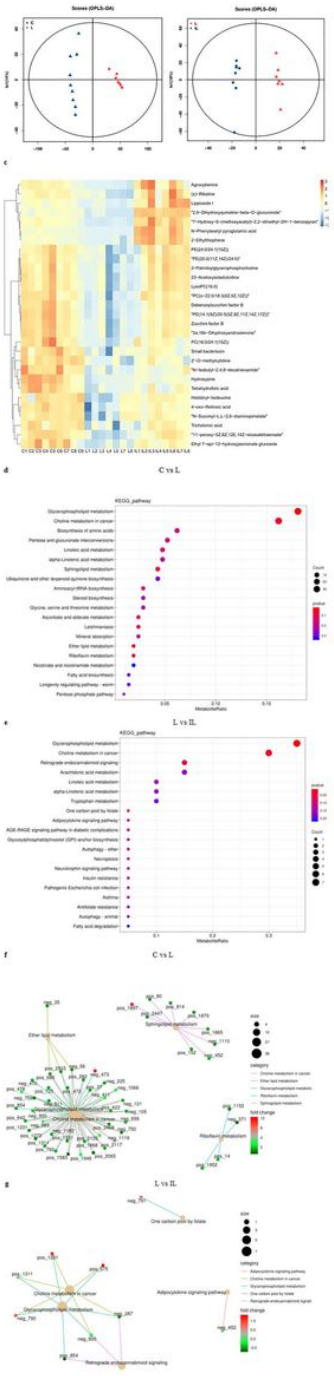

Figure 4

The alteration of serum metabolites. a OPLS-DA of serum metabolites in C vs. L. b OPLS-DA of serum metabolites in L vs. IL. c The heatmap of overlapping DMs of C vs. L and L vs. IL. d KEGG enriched pathways of the significantly altered serum metabolites in C vs. L. e KEGG enriched pathways of significantly altered serum metabolites in L vs. IL. f KEGG enriched pathways of correlation network plot in C vs. L. h KEGG enriched pathway of correlation network plot in L vs. IL. C: control group; I: I3C group; L: LPS group; IL: I3C+LPS group.

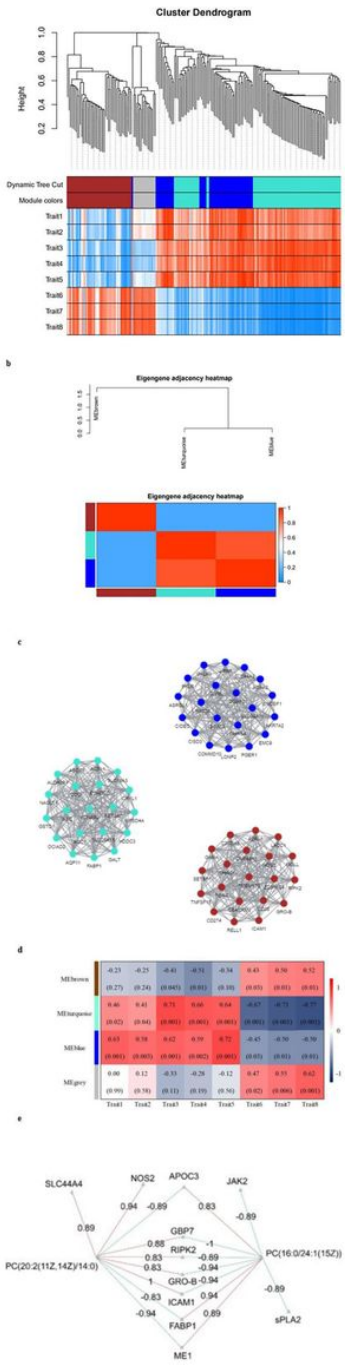

Figure 5

WGCNA results of 8 DMs (8 traits) with 194 DEGs. a WGCNA module plot showed four different modules (MEblue, MEbrown, MEturquoise, MEgrey) with different colors (blue, brown, turquoise, grey). b WGCNA module correlation plot of MEblue, MEbrown and MEturquoise. c Network visualization of WGCNA hub genes of three modules. d The plot of WGCNA module trait correlation. The values in boxes represent the Pearson's correlation coefficient between the modules with glycerophospholipids and the numbers in parentheses below Pearson's correlation coefficient represent the P-value. The red color and blue color show positive and negative correlation, respectively. e The correlation network plot of immune regulatory genes with glycerophospholipids. C: control group; I: I3C group; L: LPS group; IL: I3C+LPS group.

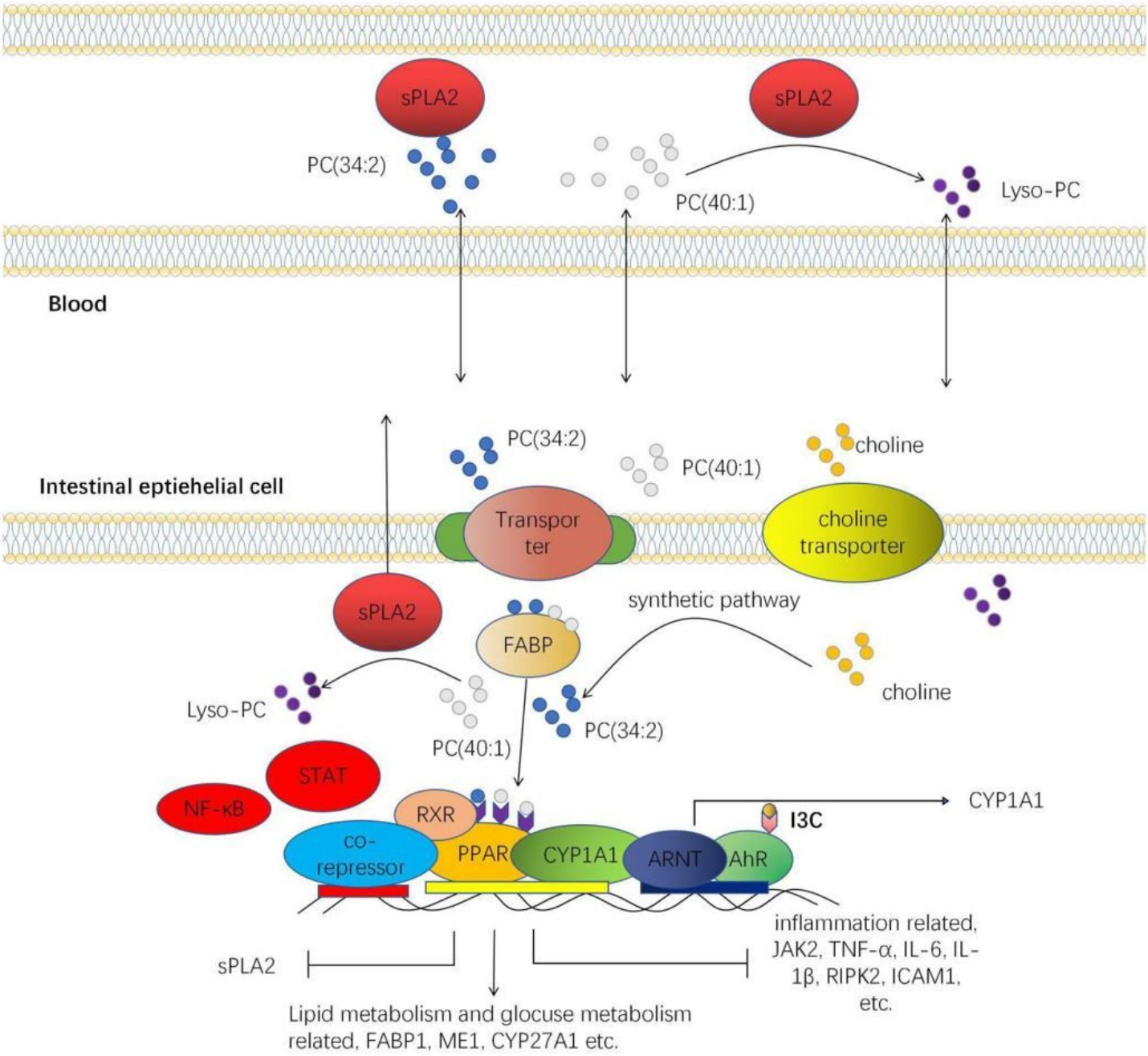

Figure 6

I3C mediated the attenuation of inflammation and recovery of metabolic disorders through the PPAR signaling pathway. LPS increased the expression of pro-inflammatory cytokines (TNF-α, IL-6, IL-1β, ICAM1, NOS2), key genes of the inflammatory pathway (RIPK2 and JAK2), secretory phospholipase A2 (sPLA2) and choline transporter (SLC44A4). sPLA2 regulated the hydrolysis of PC (16:0/24:1(15Z)), and SLC44A4 was related with the synthesis of PC (20:2(11Z,14Z)/14:0). I3C improved metabolism and biosynthesis, and thus recovered the serum concentrations of PC (16:0/24:1(15Z)) and PC (20:2(11Z,14Z)/14:0) downregulated by LPS. PPAR signaling pathway mediated anti-inflammatory effects through the suppression of NF-κB and STAT binding to DNA reaction element sequence, and PPAR was activated by CYP1A1 and PC (16:0/24:1(15Z)) upregulated by I3C. PC (20:2(11Z,14Z)/14:0) may have a pro-inflammatory effect. PC(34:2): PC (20:2(11Z,14Z)/14:0); PC(40:1): PC (16:0/24:1(15Z))

Supplementary Files

This is a list of supplementary files associated with this preprint. Click to download.

- Supplementarymeterial.docx